Title: Intracellular pH regulates β-catenin with low pHi increasing adhesion and signaling functions

Condensed title: pH regulates β-catenin stability to alter function

Authors: Brandon J. Czowski[1,2] and Katharine A. White[1,2]

Affiliations:

[1]Department of Chemistry and Biochemistry, University of Notre Dame

[2]Harper Cancer Research Institute, University of Notre Dame

Summary:

Intracellular pH (pHi) regulates the degradation rate of the pH sensor β-catenin, altering protein abundance, localization, and function in epithelial cells. This work shows pHi acts as a rheostat to alter both adhesion and signaling functions of β-catenin.

Abstract:

Intracellular pH (pHi) dynamics are linked to cell processes including proliferation, migration, and differentiation. The adherens junction (AJ) and signaling protein β-catenin has decreased abundance at high pHi due to increased proteasomal-mediated degradation. However, the effects of low pHi on β-catenin abundance and functions have not been characterized. Here, we show that low pHi stabilizes β-catenin in epithelial cells using population-level and single-cell assays. β-catenin abundance is

increased at low pHi and decreased at high pHi. We also assay single-cell protein degradation rates to show that β-catenin half-life is longer at low compared to high pHi. Importantly, we show that AJs are not disrupted by β-catenin loss at high pHi due to rescue by plakoglobin. Finally, we show that low pHi increases β-catenin transcriptional activity in single cells and is indistinguishable from a Wnt-on state. This work characterizes pHi as a rheostat regulating β-catenin abundance, stability, and function and implicates β-catenin as a molecular mediator of pHi-dependent cell processes.

Introduction

Spatiotemporal pHi dynamics regulate cell processes like differentiation (Ulmschneider et al., 2016), cell migration (Denker and Barber, 2002), cell cycle progression (Spear and White, 2023), and cell fate determination (Liu et al., 2023). While low pHi is required to maintain the adult stem cell niche (Liu et al., 2023; Ulmschneider et al., 2016) and transient increases in pHi are required for successful differentiation (Ulmschneider et al., 2016), the molecular drivers of these pHi-dependent processes are unknown. Recent work has identified β-catenin as a pH-sensitive protein with decreased abundance at high pHi driven by pH-dependent binding of β-catenin to the E3 ligase, β-transducin repeat containing protein (β-TrCP) (White, Katharine A.; Grillo-Hill, Bree K.; Esquivel, Mario; Peralta, Jobelle; Bui, Vivian N.; Chire, Ismahan; Barber, 2018).

β-catenin is a multifunctional protein that serves both structural and transcriptional roles inside cells, maintaining adherens junctions (AJs) between

47 epithelial cells and functioning as the main signal transducer of the Wnt pathway
48 (Perez-Moreno and Fuchs, 2006; Vleminckx et al., 1999; Wodarz and Nusse, 1998).
49 Co-localization of β-catenin and E-cadherin at AJs is crucial for AJ integrity (Chen et al.,
50 1999), protects E-cadherin from degradation (Huber et al., 2001), and recruits α-catenin
51 to bridge AJs and the cytoskeleton (Drees et al., 2005). In the absence of Wnt ligand,
52 cytoplasmic β-catenin is bound and degraded by a destruction complex composed of
53 Axin, Adenomateous polyposis coli (APC), casein kinase 1 α (CK1α), glycogen
54 synthase kinase 3-β (GSK3β), and β-TrCP (Nusse and Clevers, 2017). Obligate
55 phosphorylation of β-catenin by CK1α and GSK3β target β-catenin for degradation (Yost
56 et al., 1996) by the proteasome (Hart et al., 1999). In the Wnt-on case, the destruction
57 complex is sequestered, reducing kinase activity and dissociating β-TrCP (MacDonald
58 et al., 2009; Mukherjee et al., 2018). Unphosphorylated β-catenin accumulates in the
59 cytoplasm and translocates to the nucleus to displace Groucho from the transcriptional
60 repressive complex (Groucho/TCF/LEF) and forms a transcriptionally active complex (β-
61 catenin/TCF/LEF) (Daniels and Weis, 2005). This active complex promotes the
62 expression of several proliferative and morphogenic genes, such as cyclin D1 (Tetsu
63 and McCormick, 1999), c-myc (He et al., 1998), and SLUG (Moon et al., 2021).
64
65 While White et al. previously showed that high pHi was sufficient to reduce whole
66 cell and junctional β-catenin abundance in the *Drosophila* eye epithelia and in normal
67 mammalian epithelial cells (White, Katharine A.; Grillo-Hill, Bree K.; Esquivel, Mario;
68 Peralta, Jobelle; Bui, Vivian N.; Chire, Ismahan; Barber, 2018), there were several
69 significant limitations to this prior work. First, the effect of low pHi on β-catenin

70 abundance was not explored due to the lack of methods for reliably lowering pHi in
71 epithelial cells. Second, the effects of pHi-mediated β-catenin abundance changes on
72 the integrity and composition of AJs were not completely characterized. Third, the pH-
73 dependent transcriptional activity of endogenous β-catenin was not investigated. Thus,
74 our understanding of how pHi regulates β-catenin function is incomplete. Given the
75 context-dependent function of β-catenin, a full characterization of pH-dependent
76 abundance of all subcellular pools (nuclear, cytoplasmic, junctional) is needed.
77
78 Here, we have developed methods to both raise and lower pHi in Madin Darby
79 Canine Kidney cells and assay pH-dependent effects on β-catenin abundance, sub-
80 cellular localization, and degradation dynamics. This enables us to investigate how both
81 increased and decreased pHi alters the abundance, degradation dynamics, and
82 functions of β-catenin. Using population level immunoblots we demonstrate pH-
83 dependent β-catenin abundance, with increased abundance at low pHi compared to
84 high pHi. We also characterize abundance of distinct subcellular pools of β-catenin
85 using immunofluorescent microscopy. We show that nuclear, cytoplasmic, and junctional
86 β-catenin pools are all decreased at high pHi while low pHi stabilizes both nuclear and
87 cytoplasmic pools of β-catenin. We also used a photoconvertible mMaple3-β-catenin
88 fusion to determine pH-dependent β-catenin degradation dynamics in single cells. We
89 showed that low pHi increases β-catenin half-life while high pHi reduces β-catenin half-
90 life. Collectively, our data demonstrate that pHi regulates β-catenin degradation rates by
91 functioning as a rheostat to modulate β-catenin abundance.
92

93 Importantly, our work also characterizes how pHi regulates β-catenin function by
94 identifying pH-dependent AJ composition where β-catenin is enriched at low pHi in E-
95 cadherin containing AJs. High pHi resulted in the loss of β-catenin at E-cadherin
96 containing AJs but recruitment of plakoglobin maintained AJ integrity and epithelial
97 morphology. We also demonstrate that modest (~10%) increases in nuclear abundance
98 of β-catenin at low pHi were sufficient to significantly increase β-catenin transcriptional
99 activity, phenocopying transcriptional activation observed with activation of the Wnt
100 pathway. Our results demonstrate that pHi functions as a rheostat to regulate the
101 abundance, stability, and function of endogenous wild-type β-catenin. This work will
102 improve our understanding of both normal biological processes (differentiation) and
103 pathological processes (transformation, cancer stem cells) that are marked by temporal
104 changes in pHi (Liu et al., 2020; Ulmschneider et al., 2016; White et al., 2017).
105

106 **Results**

107 *Intracellular pH differentially affects subcellular pools of β-catenin*

108 To investigate the pH-dependent regulation of β-catenin in a mammalian cell
109 model, we used Madin-Darby canine kidney (MDCK) cells. β-catenin has been
110 extensively studied in MDCK cells, where it was previously shown that increased pHi
111 was sufficient to reduce overall β-catenin abundance at the population level as well as
112 nuclear and junctional pools at the single cell level (White et al., 2018). This prior work
113 established a role for high pHi in regulating β-catenin abundance; however, the lack of
114 methods to lower pHi in this cell line prevented complete characterization of the role of
115 pHi in regulating β-catenin abundance, localization, and function.

116 We first developed a new approach to experimentally lower pHi in MDCK cells,
117 using a combination treatment of a sodium-proton exchanger 1 (NHE1) inhibitor (5-(N-
118 ethyl-N-isopropyl)amiloride (EIPA)) and a sodium-bicarbonate cotransporter (NCBn1)
119 inhibitor (2-chloro-N-[[2′-[(cyanoamino)sulfonyl][1,1′-biphenyl]-4-yl]methyl]-N-[(4-
120 methylphenyl)methyl]-benzamide (S0859)) (Larsen et al., 2012). To experimentally raise
121 pHi, we used 15% CO_2 atmospheric culture conditions, which increases the bicarbonate
122 concentration in the culturing medium and, through the function of NCBn1, results in
123 increased intracellular bicarbonate and increased pHi (White et al., 2018). Basal pHi in
124 control MDCK cells was measured at 7.36±0.02, while pHi manipulation treatments
125 were able to significantly increase pHi to 7.49±0.10 (15% CO_2) or significantly decrease
126 pHi to 7.17±0.05 (EIPA+S0859) after 24 hours (Figure 1A). Together, these
127 manipulation methods enable us to study how physiological changes in pHi of 0.13-0.32
128 pH units regulate β-catenin. These pHi changes are physiologically relevant as pHi
129 dynamics of similar magnitude occur during cellular differentiation (+0.2 pH units)
130 (Ulmschneider et al., 2016) and cell division (+0.25 pH units) (Spear and White, 2023).
131 Importantly, the presence of the proteosome inhibitor MG132 (Lee and Goldberg, 1996)
132 did not affect the pHi changes achieved with these manipulation protocols (Figure 1A).
133 We also verified that the treatments used to manipulate pHi for 24 hours did not alter
134 cell viability (Figure S1). Together, these conditions allow us to study roles for increased
135 and decreased pHi on β-catenin abundance.
136 We next used western blot approaches to assay β-catenin abundance at high
137 and low pHi. We did confirm that high pHi decreased β-catenin abundance compared to
138 control and we showed that low pHi was sufficient to stabilize β-catenin abundance

compared to high pHi (Figure 1 B&C). Importantly, we demonstrated that pH-dependent abundance of β-catenin is regulated by proteosome—mediated degradation, as pHi manipulation in the presence of a proteasome inhibitor (MG132) abrogated pH-dependent abundance (Figure 1B&C). To ensure that low pHi was not inducing global protein stabilization, we probed the abundance of the AJ protein, E-cadherin (Figure 1D). We found that high and low pHi conditions had no effect on the overall abundance of E-cadherin (Figure 1E), demonstrating that the pH-dependent changes in β-catenin abundance does not result from global protein degradation or stabilization. These data suggest that pHi functions as a rheostat in regulating β-catenin abundance at the population level, with increased stability at low pHi compared to high pHi.

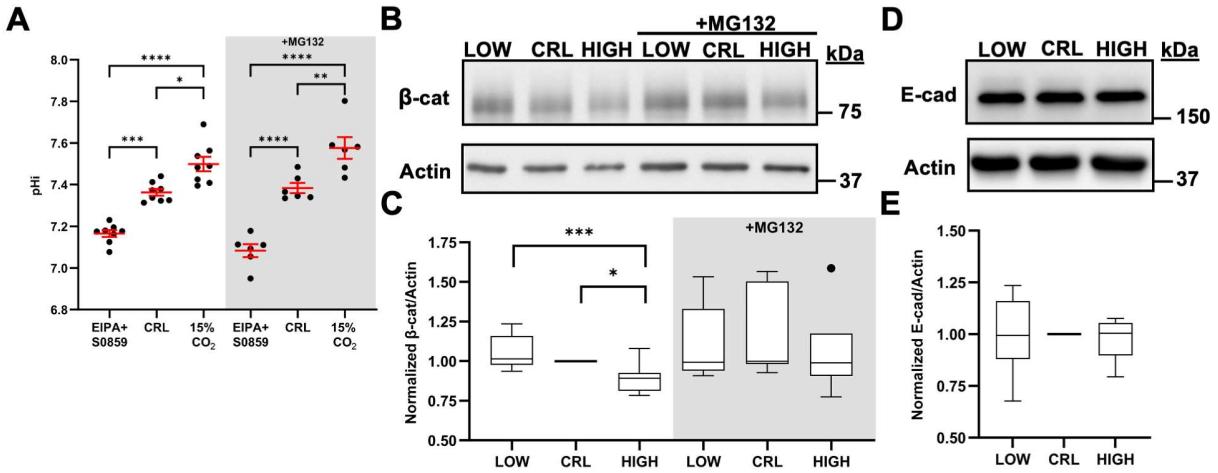

Figure 1: Decreased pHi stabilizes β-catenin abundance through a proteosome-dependent mechanism. (A) Box and whisker plots showing population level pHi measurements in MDCK cells after 24-hour treatments with 1 μM EIPA+ 30 μM S0859 (low) or 15% CO_2 (high) to lower and raise pHi, respectively. Mean and SEM shown. n=6-8. **(B)** Representative immunoblot of β-catenin (β-cat) and actin under low, control, and high pHi conditions in the presence and absence of proteosome inhibition (MG132). **(C)** Quantification of β-catenin immunoblot data collected as described in **(B)**. Individual biological replicates were normalized to control MDCK within each experiment. Box and whisker plots show median (line), 25th-75th percentile (boxes), min and max (whiskers), and outlier values with points. n=6-8. **(D)** Representative immunoblot of E-cadherin and actin under low, control, and high pHi conditions. **(E)** Quantification of E-cadherin

162 immunoblot data collected as described in **(D)** and displayed and normalized as
163 described in **(C)**. n=6. Statistical analyses in **(A)** were determined using one-way
164 ANOVA test with Sidak's correction for multiple comparisons. Statistical analyses in **(C)**
165 and **(E)** were determined with ratio paired t-tests between treatment groups and one-
166 sample t-tests with a hypothetical mean of 1.0 when comparing to control (which had no
167 variation due to normalization). *P<0.05; **P<0.01 ***P<0.001; ****P<0.0001.
168

169 Because the function of β-catenin is determined by its subcellular localization,
170 phosphorylation state, and availability of binding partners (Krieghoff et al., 2006; Morgan
171 et al., 2019; Valenta et al., 2012), we next investigated how pHi alters the abundance
172 and distribution of each subcellular pool of β-catenin. We first confirmed that the pHi
173 manipulation techniques altered pHi in single MDCK cells using live-cell, confocal
174 microscopy and nigericin standardization (Grillo-Hill et al., 2014; Spear and White,
175 2023) (Figure S2A). We found that under control conditions the median pHi value of
176 MDCK cells was 7.39±0.14 (Figure S2B), in line with the previous calculations using
177 population-level measurements. Importantly, treatment with EIPA+S0859 significantly
178 lowered single-cell pHi to 7.26±0.17, whereas treatment with 15% CO_2 significantly
179 raised pHi to 7.42±0.20, relative to control MDCK cells (Figure S2B).

180 We hypothesized that high pHi would decrease β-catenin levels in each
181 subcellular pool, whereas low pHi would stabilize each subcellular pool. This hypothesis
182 is predicated on recent data suggesting subcellular pools of β-catenin can rapidly
183 exchange and are regulated by the availability of subcellular binding partners (Krieghoff
184 et al., 2006; Morgan et al., 2019). To test this hypothesis, we developed a 3D image
185 analysis pipeline to segment normal epithelial cells (MDCK) and separately measure β-
186 catenin abundance in the nucleus, cytoplasm, and at adherens junctions (Figure S3,
187 see methods). Briefly, cytoplasmic and nuclear regions of interest were generated in

188 Nikon Imaging Software-Elements (NIS-Elements), using Hoechst dye (DNA) to identify
189 nuclear boundaries and an E-cadherin antibody (adherens junctions) to identify cell
190 boundaries (Figure S3). To specifically quantify junctional pools of β-catenin, we used
191 IMARIS (Oxford Instruments, see methods) software to generate 3D surfaces
192 representative of adherens junctions where E-cadherin was used as a marker of
193 adherens junctions.

194 Using this segmentation procedure, we quantified β-catenin abundance in each
195 subcellular pool (cytoplasmic, nuclear, junctional) after 24 hours of pHi manipulation
196 (Figure 2A). We found that all subcellular pools of β-catenin decreased at high pHi
197 (Figure 2B), which agrees with the population-level western blot data, and our
198 hypothesis of increased pHi being sufficient to reduce β-catenin abundance across all
199 subcellular pools. This data is also in agreement with prior quantification of β-catenin
200 abundance at junctions and in the nucleus of MDCK cells maintained at high pHi (White,
201 Katharine A.; Grillo-Hill, Bree K.; Esquivel, Mario; Peralta, Jobelle; Bui, Vivian N.; Chire,
202 Ismahan; Barber, 2018). At low pHi, we found that the cytoplasmic and nuclear pools of
203 β-catenin were significantly increased compared to control and high pHi conditions
204 (Figure 2A&B). In our initial analysis, low pHi was not sufficient to increase the total
205 abundance of β-catenin at adherens junctions compared to control MDCK cells (Figure
206 2B). However, contrary to our population level measurements (Fig 1C), we observed a
207 significant decrease in E-cadherin at MDCK junctions under low pHi compared to
208 control MDCK (Fig 2A&C). Importantly, this loss of E-cadherin at low pHi does not alter
209 cell morphology. We further quantified the ratio of β-catenin to E-cadherin at MDCK
210 junctions and observed strong pH-dependence with increased β-catenin localizing in E-

211 cadherin-containing AJs at low pHi compared to control and high pHi (Fig 2D). This
212 suggests that the level of β-catenin saturation at AJs changes with pHi, with less β-
213 catenin in E-cadherin-containing AJs at high pHi and more β-catenin in E-cadherin-
214 containing AJs at low pHi, even as total junctional E-cadherin is reduced.

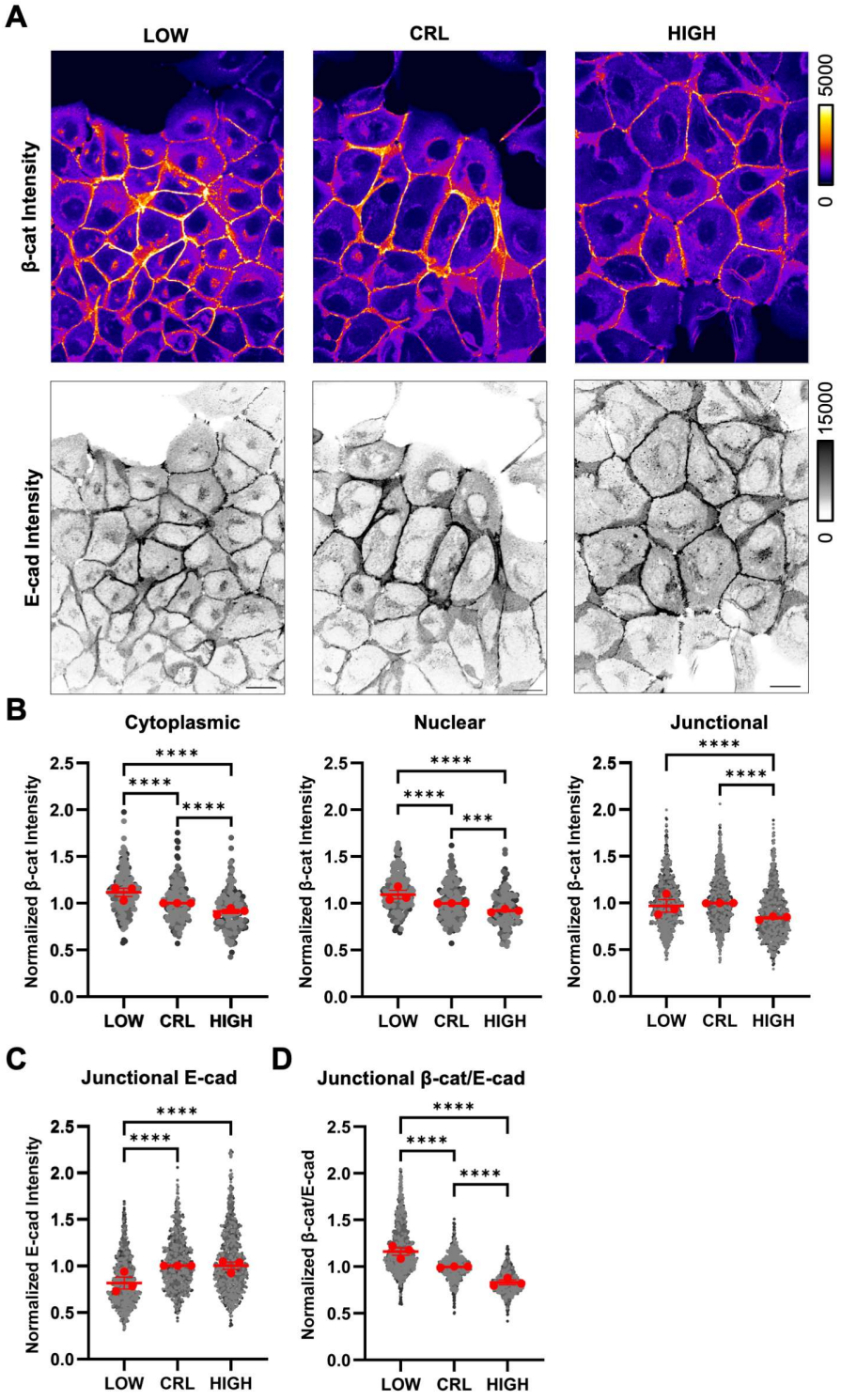

Figure 2: β-catenin abundance across subcellular pools is differentially regulated by pHi. (A) Representative confocal images of MDCK cells fixed and stained for β-catenin (β-cat) and E-cadherin (E-cad). β-catenin is pseudocolored and E-cadherin is shown in inverse mono according to each scale. Scale bar: 20 μM. **(B)** Quantification of cytoplasmic, nuclear, and junctional pools of β-catenin. Individual cells and surfaces

were normalized to the median of control conditions within each biological replicate. Individual cytoplasms, nuclei, and junctions are shown as gray dots with various shading for each biological replicate. Red dots represent the median for each biological replicate with interquartile ranges shown with bars. **(C)** Quantification of junctional E-cadherin displayed and normalized as in **(B)**. **(D)** Calculation of β-cat/E-cad ratio from quantifications in **(B)** and **(C)** that are normalized and displayed as in **(B)**. Individual cytoplasms and nuclei, n=171-221; junctions, n=934-1194, from 3 biological replicates. Statistical analyses in **(B-D)** were performed using the Kruskal-Wallis test with Dunn's multiple comparison correction. ***P<0.001, ****P<0.0001.

Taken together, our data suggest that subcellular pools of β-catenin are exchangeable, where high pHi causes cytoplasmic pools to be reduced, resulting in concomitant loss of nuclear and junctional β-catenin. Similarly, our data suggest low pHi results in cytoplasmic and nuclear accumulation and a relative increase in β-catenin at E-cadherin containing AJs. Collectively, these data demonstrate that manipulating pHi for 24 hours in MDCK cells significantly alters β-catenin abundance in single cells. Quantification of each subcellular pool of β-catenin under each condition provides the first glimpse as to how β-catenin distribution and abundance change with respect to pHi dynamics.

Endogenous plakoglobin compensates for pHi-dependent loss of β-catenin to maintain AJs at high pHi

In the immunofluorescence assays of β-catenin, we observed no change in MDCK colony morphology with altered pHi, even when junctional pools of β-catenin were significantly decreased at high pHi (Figure 2A&B). This suggests that other AJ proteins may be able to rescue the loss of junctional β-catenin to maintain AJ integrity. While β-catenin is well-known for maintaining AJs, plakoglobin serves adhesive functions in both AJs and desmosomes, with preferential incorporation into the latter

249 (Cowin et al., 1986). Work by Fukunaga and colleagues demonstrated the functional
250 redundancy of β-catenin and plakoglobin in maintaining AJs, where cell-cell contacts
251 can be rescued with plakoglobin expression in a β-catenin null background (Fukunaga
252 et al., 2005). Furthermore, knockout of β-catenin in mouse models resulted in significant
253 recruitment of plakoglobin to AJs, compensating for the loss of β-catenin (Wickline et al.,
254 2011). A similar effect was observed in mouse models using conditional β-catenin
255 knockdown in cardiomyocytes, where β-catenin was reduced by 90% and plakoglobin
256 was subsequently enriched at junctions (Zhou et al., 2007). We therefore hypothesized
257 that in MDCK cells, the homologous protein plakoglobin can rescue β-catenin loss at
258 junctions at high pHi to preserve epithelial morphology.
259
260 To determine whether plakoglobin compensates for the pHi-dependent loss of β-
261 catenin from AJs at high pHi, we performed immunofluorescent confocal microscopy of
262 plakoglobin using the same segmentation pipeline outlined in Figure S3 after 24 hours
263 of pHi manipulation. We found that junctional plakoglobin was significantly increased at
264 high pHi and significantly decreased at low pHi compared to control MDCK (Figure
265 S4A&B). Importantly, overall abundance of plakoglobin is unchanged by pHi (Figure
266 S4C). In summary, while β-catenin co-localization with E-cadherin is reduced at high pHi
267 compared to control (Figure 2D), plakoglobin co-localization with E-cadherin is
268 increased at high pHi (Figure S4B). This suggests that when β-catenin is lost from
269 junctions at high pHi, plakoglobin is recruited to stabilize AJs and attenuate morphology
270 changes due to β-catenin loss.
271

272 *Characterization of pH-dependent β-catenin degradation*

273 Prior work has already extensively examined roles for high pHi in reducing β-
274 catenin stability (White, Katharine A.; Grillo-Hill, Bree K.; Esquivel, Mario; Peralta,
275 Jobelle; Bui, Vivian N.; Chire, Ismahan; Barber, 2018), but the effects of low pHi on β-
276 catenin stability has not been characterized. We next measured the temporal
277 localization and stability dynamics of endogenous β-catenin, with the prediction that low
278 pHi increases β-catenin stability resulting in the observed increased β-catenin
279 abundance at low pHi. We quantified pH-dependent stability of β-catenin by performing
280 a cycloheximide chase assay (Kao et al., 2015) after 24 hours of pHi manipulation in
281 MDCK cells, collecting samples every 30 minutes for 2.5 hours (Figure S5A). The half-
282 life of endogenous β-catenin was determined to be 1.58 hours in control MDCK cells, in
283 agreement with prior work in MDCK cells (White et al, 2018). Importantly, we found that
284 β-catenin half-life was increased at low pHi (2.79 hours) and decreased at high pHi
285 (1.22 hours) compared to control (Figure S5B). Of note, White et al. used different
286 treatment conditions to raise pHi (ammonium chloride compared to our method of 15%
287 CO_2) (Whtie et al, 2018). Thus, our work indicates that high pHi accelerates β-catenin
288 degradation, regardless of the method of pHi manipulation. Finally, this work is the first
289 to report an extension of β-catenin half-life in cells under low pHi conditions.

290

291 *An experimental approach to monitor β-catenin degradation rates in single cells*

292 The population-level analyses of β-catenin stability using cycloheximide
293 demonstrated pH-dependence, where low pHi increased and high pHi decreased β-
294 catenin half-life relative to control. Although these data revealed altered rates of β-

295 catenin degradation with pHi manipulation, the population data require discontinuous
296 measurements across cell populations and lack both single-cell and temporal resolution.
297 Single-cell analyses are important for answering biological questions, particularly for
298 elucidating roles for pH-dependent β-catenin regulation in pH-dependent processes that
299 occur at the single-cell level, such as differentiation (Ulmschneider et al., 2016). One
300 approach for quantifying live- and single-cell protein dynamics is through monitoring a
301 photoconvertible fluorescent protein (PCFP) fused to a protein of interest. PCFPs are a
302 subfamily of fluorescent proteins that undergo an excitation and emission spectra shift
303 upon stimulation with a specific wavelength of light (Shcherbakova and Verkhusha,
304 2014). This approach enables the photoconversion of a small subpopulation of the
305 PCFP-tagged protein, allowing for specific tracking of the photoconverted protein
306 fluorescence intensity as a direct readout of protein localization changes and
307 degradation (after accounting for photobleaching effects). This approach also eliminates
308 the need to average bulk cell responses as with cycloheximide chase assays, while
309 investigating how pHi regulates protein degradation in single cells.
310 We selected mMaple3, a PCFP that transitions from green-to-red fluorescence
311 upon exposure to 405 nm light, for these assays to monitor live-cell β-catenin protein
312 degradation rates. Derived from the parent protein mMaple, mMaple3 has reduced
313 dimerization tendency, superior brightness in the converted channel, and improved
314 photoconversion efficiency (defined as the proportion of protein that yields detectable
315 fluorescence signal) (McEvoy et al., 2012; Wang et al., 2014; Zhang et al., 2007). To
316 validate that we could measure differences in protein degradation rates of
317 photoconverted mMaple3 using confocal microscopy, we transiently expressed

318 mMaple3 alone or N-terminally fused to β-catenin (mMaple3-β-catenin) and determined
319 fitted half-life values of median cell traces to compare relative protein stability. This
320 assay does not permit determination of the absolute half-life of β-catenin, as loss of
321 fluorescent signal includes protein degradation, diffusion, and photobleaching of the
322 PCFP. However, this approach does allow us to compare relative degradation rates
323 across conditions. In MDCK cells expressing mMaple3 alone, the half-life was >1201
324 seconds, while the half-life of mMaple3-β-catenin was significantly reduced to just 290.9
325 seconds (Figure S6). This suggests that the shorter mMaple3-β-catenin half-life is being
326 driven by ubiquitination and degradation of β-catenin in the fusion protein. Confirming
327 this, we showed that treatment with proteasome inhibitor (MG132) significantly
328 increased the half-life of mMaple3-β-catenin to 686.9 seconds (Figure S6). Taken
329 together, these data demonstrate mMaple3-β-catenin is i) degraded much faster than
330 mMaple3 alone and ii) can be stabilized by inhibiting proteasome activity. Thus, using
331 this single-cell system we can monitor mMaple3-β-catenin degradation dynamics in
332 single cells and compare relative half-life values between conditions. Next, we
333 measured mMaple3-β-catenin degradation rates under pHi manipulation conditions in
334 single MDCK cells.
335
336 *Intracellular pH titrates the degradation rates of β-catenin in single epithelial cells*
337 We altered pHi in mMaple3-β-catenin expressing MDCK cells and
338 photoconverted cytoplasmic mMaple3-β-catenin using a spatially restricted region of
339 interest (Supplemental Video 1). We then monitored relative degradation rates of
340 cytoplasmic β-catenin in single cells (Figure 3A) and observed a reduced median half-

life at high pHi (200.2 seconds) and increased median half-life at low pHi (294.4 seconds) compared to control MDCK cells (263.4 seconds). Importantly, this approach allows us to determine mMaple3-β-catenin half-life in individual cells. We similarly found that cells with low pHi had significantly stabilized mMaple3-β-catenin compared to high pHi MDCK cells (Figure 3B). These experiments demonstrate that pHi titrates the degradation rate of cytoplasmic β-catenin in single cells, with faster degradation at high pHi and slower degradation at low pHi compared to control.

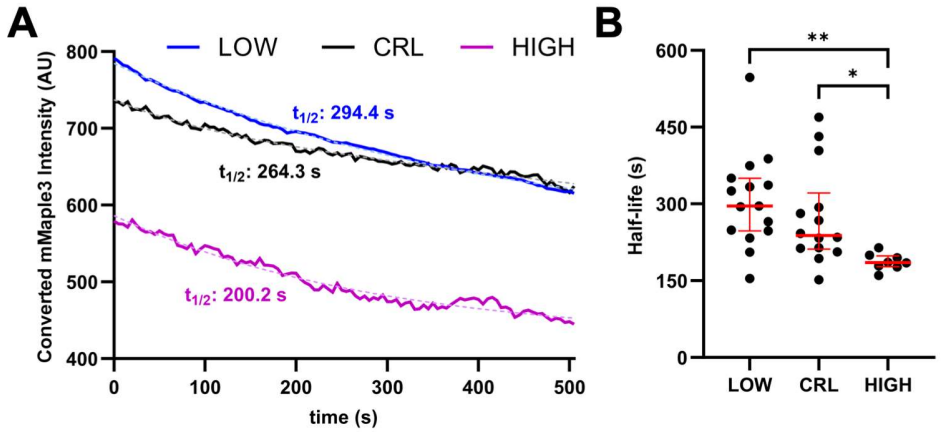

Figure 3: mMaple3-β-catenin can be used to compare relative degradation rates of β-catenin that are regulated by pHi. (A) Raw median cell traces for each condition were fit using nonlinear regression to obtain half-life values. LOW, n=14; CRL, n=13; HIGH, n=11; N=3. **(B)** Single-cell half-life values were obtained by fitting individual cell traces as in **(A)**. Median shown as line with interquartile range shown as bars. Outliers were removed using the ROUT method (Q=1%). LOW, n=14; CRL, n=13; HIGH, n=8 from 3 biological replicates. Statistical significance in **(B)** was determined using Kruskal-Wallis test with Dunn's correction for multiple comparisons. *P<0.05, **P<0.01.

In the photoconversion experiments described above, we performed cytoplasmic photoconversion and specific tracking of the cytoplasmic pool. This approach also allows us to monitor subcellular redistribution of photoconverted cytoplasmic mMaple3-β-catenin into the nucleus. We measured nuclear accumulation of photoconverted

363 mMaple3-β-catenin following cytoplasmic photoconversion and observed significantly
364 increased nuclear accumulation of mMaple3-β-catenin at low pHi compared to high pHi
365 cells (Figure S7). These data suggest that pHi modulates nuclear accumulation of
366 photoconverted β-catenin and supports the observation that nuclear β-catenin
367 abundance is increased at low pHi compared to control and high pHi (Figure 2B). While
368 the function of β-catenin is regulated by its localization, recent work revealed that
369 nuclear localization alone is not sufficient to determine β-catenin function (Van Der Wal
370 and Van Amerongen, 2020). Our work suggests that low pHi significantly increases β-
371 catenin abundance in the cytoplasm and nucleus from attenuated degradation in the
372 cytoplasm. A remaining unanswered question is whether the transcriptional activity of
373 wild-type, endogenous β-catenin is altered as a consequence of pH-dependent
374 degradation of cytoplasmic protein pools, as this was not addressed in prior work
375 investigating pH-dependent β-catenin stability (White, Katharine A.; Grillo-Hill, Bree K.;
376 Esquivel, Mario; Peralta, Jobelle; Bui, Vivian N.; Chire, Ismahan; Barber, 2018). To
377 address this, we tested the hypothesis that low pHi increases the transcriptional activity
378 of β-catenin whereas high pHi reduces transcriptional output.
379
380 *Decreased pHi is sufficient to increase transcriptional activity of β-catenin*
381 We first used population-level reverse transcriptase quantitative polymerase
382 chain reaction (RT-qPCR) of endogenous β-catenin transcriptional targets after 24
383 hours of pHi manipulation in MDCK cells. We identified MYC and SLUG as direct
384 transcriptional targets of β-catenin and verified primer specificity of each target (see
385 Methods) (Martínez-Estrada et al., 2006). At low pHi we found an increase in transcript

386 abundance for MYC and SLUG, while high pHi resulted in a decrease for each of these
387 targets (Figure S8). Similarly to the population-level β-catenin abundance analysis, we
388 only observed a modest pH-dependent trend for each target (Figure S8). Therefore, we
389 next compared the level of β-catenin transcriptional activity achieved at low pHi to an
390 active Wnt-on cell state. Stimulation of MDCK cells with WNT3a ligand for 24 hours
391 resulted in a similar increase of MYC and SLUG transcript abundance that observed
392 under low pHi conditions (Figure S8). Importantly, the observed level of pathway
393 activation agrees with the magnitude of response previously observed in WNT3a
394 stimulated MDCK cells (Howard et al., 2011). These data suggest that low pHi is
395 sufficient to induce β-catenin transcriptional activation that is indistinguishable from
396 WNT3a stimulation in MDCK cells.

397 A recent study has shown that Wnt activity is heterogenous within a tumor, and
398 single-cell analysis of Wnt pathway activation correlated with higher expression of target
399 genes (Yi et al., 2020). Thus, we reasoned that Wnt activation may be heterogenous
400 even in a clonal population of MDCK cells. To investigate this, we next performed
401 single-cell analysis of pH-dependent β-catenin transcriptional activity using a highly
402 specific LEF-1/TCF transcriptional reporter plasmid that drives expression of
403 destabilized GFP (TOPdGFP) (Reya et al., 2003). Cells transiently expressing the
404 plasmid were treated with pHi manipulation media for 24 hours prior to live-cell imaging
405 using confocal microscopy (Figure 4A). The single-cell transcriptional response was
406 heterogeneous in clonal normal epithelial cells, but we observed a statistically
407 significant increase in reporter fluorescence at low pHi compared to high pHi (Figure
408 4B). We again compared the extent of pH-dependent signaling upregulation to MDCK

409 cells treated with WTN3a. We found that WNT3a treatment resulted in an increase in
410 reporter intensity compared to control MDCK and that the extent of reporter transcription
411 with low pHi was statistically indistinguishable from Wnt3a (Figure 4A&B). These single-
412 cell analyses show that low pHi alone can recapitulate the Wnt-active state, highlighting
413 low pHi as a driver of β-catenin transcriptional activity in normal epithelial cells.

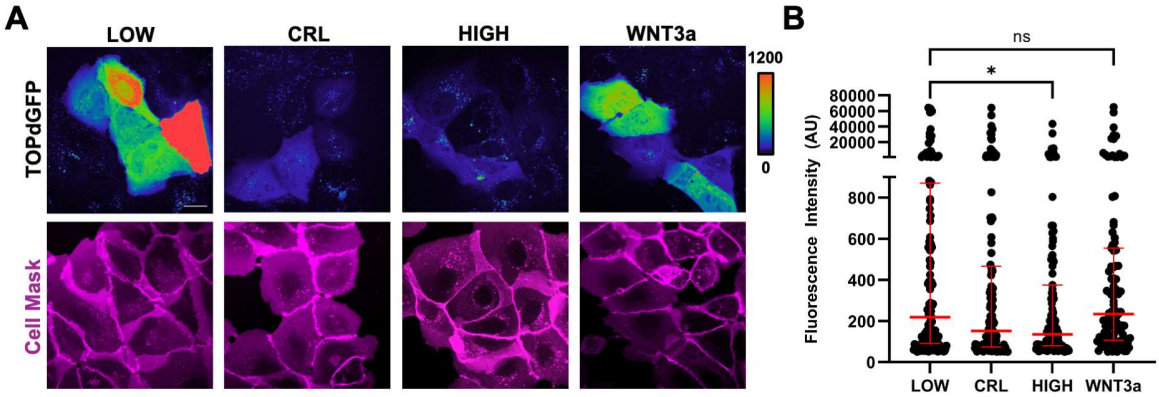

Figure 4: Low pHi phenocopies WNT3a-mediated activation of β-catenin transcription. (A) Representative images of MDCK cells expressing a TOPdGFP reporter plasmid shown according to scale with cell membranes visualized with Cell Mask (magenta). Scale bar = 20μm. **(B)** Quantification of single-cell reporter intensities after 24 hours of pHi manipulation or WNT3a treatment (40 ng/mL). All cells in each field of view were quantified and were plotted if the average intensity was two-fold higher than the average of mock-transfected cells. Individual cells are shown as block dots with median and interquartile ranges shown in red lines and bars, respectively. LOW, n=103, N=5; CRL, n=181, N=7; HIGH, n=147, N=5; WNT3a, n=103, N=3. Statistical significance in **(B)** was determined using Kruskal-Wallis test with Dunn's correction for multiple comparisons. *P<0.05.

Discussion

Our data highlight an important role for pHi in serving as a rheostat to regulate β-catenin abundance, where low pHi increases β-catenin stability to promote high adhesion and transcriptional activity whereas high pHi reduces β-catenin stability to promote reduced β-catenin at AJs and lower transcriptional activity compared to control cells. This significantly expands on prior work that only explored effects of increased pHi on β-catenin abundance and did not fully characterize pH-dependent regulation of β-catenin function. Our work demonstrates how changes in pHi within the physiological range can regulate the degradation, and thus abundance and function, of endogenous β-catenin.

437 We also found that subcellular pools of β-catenin were differentially regulated by
438 pHi. We show that pHi-mediated loss of β-catenin from AJs can be rescued by
439 plakoglobin to maintain AJ integrity. While genetic knockdown of β-catenin was
440 previously shown to recruit plakoglobin to adherens junctions (Fukunaga et al., 2005),
441 here we demonstrate the pHi-mediated loss of β-catenin is sufficient to produce the
442 same compensatory phenotype at AJs.
443 Our data suggests that pHi can alter not only β-catenin membrane localization,
444 but also redistribute the cadherin and catenin composition of adherens junctions. We
445 have demonstrated the plakoglobin is able to rescue the loss of β-catenin at adherens
446 junctions under high pHi. Additionally, we have found that the composition of adherens
447 junctions changes with pHi, with a preference for β-catenin at low pHi and a preference
448 for plakoglobin at high pHi. This presents a potential novel mechanism of pH-dependent
449 AJ remodeling that may be a previously unrecognized reinforcer of pH-dependent cell
450 polarity (Frantz et al., 2007) or EMT (Amith et al., 2016). Moreover, the increased ratio
451 of plakoglobin to E-cadherin at high pHi may be indicative of changes in desmosome
452 formation, as plakoglobin-containing AJs are a prerequisite for their establishment
453 (Lewis et al., 1997). Future work investigating differences in AJ strength of
454 plakoglobin/E-cadherin and β-catenin/E-cadherin complexes will further explore how the
455 physical properties of AJ change with pHi.
456 Collectively, our population and single-cell level analyses of β-catenin
457 transcriptional activity demonstrate that modest stabilization of nuclear β-catenin is
458 sufficient to drive significant changes in transcriptional activity. We found that low pHi
459 increased β-catenin transcriptional activity and phenocopied transcriptional outcomes of

460 Wnt3a treatment. Importantly, while plakoglobin can rescue the AJ function of β-catenin
461 at high pHi, our data suggest plakoglobin cannot rescue the reduced signaling function
462 of β-catenin at high pHi. This fits with prior work showing β-catenin/TCF4 complexes are
463 transcriptionally active but that plakoglobin/TCF4 complexes are unable to bind DNA
464 (Roura et al., 1999; Simcha et al., 1998). Our data show that pHi directly regulates β-
465 catenin signaling and transcriptional activity in the absence of Wnt pathway activation
466 and indicates that pH-dependent regulation of β-catenin signaling may reinforce stem
467 cell phenotypes previously associated with low pHi (Liu et al., 2023) and high Wnt
468 signaling (Nusse, 2008).

469 Decades of research have been dedicated to understanding the dynamics and
470 regulation of β-catenin in normal physiology and disease (Nusse and Clevers, 2017;
471 Wodarz and Nusse, 1998). Our work provides new mechanistic insight in the context of
472 pH-dependent differentiation, where stem cells have low pHi and high β-catenin
473 abundance and pHi increases are necessary for differentiation, accompanied by the
474 loss of β-catenin (Fevr et al., 2007; Liu et al., 2023). Future work will explore roles for
475 pHi dynamics in regulating β-catenin abundance through pH-dependent stability to
476 support both maintenance of pluripotency (stabilized β-catenin at low pHi) and
477 facilitation of differentiation (destabilized β-catenin at high pHi).

478 Finally, our work may shed light on how pHi regulates β-catenin abundance and
479 transcriptional activity in cancer. Constitutively increased pHi is an emerging hallmark of
480 cancer that is associated with several cancer cell behaviors (White et al., 2017). While
481 pHi has been shown to increase with metastatic potential in tissue-matched cell lines
482 (Spear and White, 2023), spatial pHi heterogeneity exists in 3D cancer cell cultures

483 (Dovmark et al., 2017; Tafech et al., 2023). Concurrent work in our lab has revealed that
484 microenvironment can alter pHi and concomitantly modulate β-catenin abundance in
485 cancer cell models. In combination with these data, this work suggests that pHi changes
486 may serve as a physiological cue to regulate β-catenin abundance and activity to drive
487 transcriptional and adhesion changes associated with cancer adaptation. Future work
488 will focus on simultaneously quantifying pHi and β-catenin activity in more complex
489 models to determine if pH-dependent regulation of the Wnt pathway (through β-catenin
490 regulation) alters tumorigenic phenotypes. This will create opportunities to investigate
491 context-specific avenues for altering β-catenin abundance and regulatory pathways in
492 order to develop improved cancer therapeutics.
493
494 **Abbreviations:**
495 AJ (adherens junctions)
496 β-TrCP (Beta-Transducin repeat containing protein)
497 β-cat (Beta-catenin)
498 E-cad (E-cadherin)
499 EIPA (5-(N-ethyl-N-isopropyl)amiloride)
500 MDCK (Madin Darby canine kidney)
501 PCFP (photoconvertible fluorescent protein)
502 pHi (intracellular pH)
503 Plak (plakoglobin)
504 S0859 (2-chloro-N-[[2′-[(cyanoamino)sulfonyl][1,1′-biphenyl]-4-yl]methyl]-N-[(4-
505 methylphenyl)methyl]-benzamide)

506

507 **Materials and Methods:**

508 *Cell Culture and Conditions*

509 Madin-Darby Canine Kidney (MDCK) cells were cultured in EMEM (Quality Biological,
510 112-018-101) supplemented with 10% Fetal Bovine Serum (FBS; Peak Serum, cat: PS-
511 FB3). Cells were maintained at 37º C in a humidified incubator maintained at 5% CO_2
512 (unless indicated otherwise). Cells were authenticated and tested for mycoplasma in
513 November 2022.

514

515 *Intracellular pH manipulation*

516 Cells were plated 24 hours prior to being treated for pHi manipulation. 24 hours after
517 plating, the conditioned medium was aspirated and replaced with medium containing 1
518 μM EIPA + 30 μM S0859 (Cf) (low pHi) or fresh medium and placed in an incubator
519 maintained at 5% CO_2 (low pHi and control) or 15% CO_2 (high pHi) for 24 hours. Where
520 indicated, proteasome activity was inhibited 18 hours after pHi manipulation treatment
521 using 10 μM MG132 (Selleck, S2619) for a total of 6 hours prior to sample analysis or
522 collection.

523

524 *Acquisition and analysis of microscopy images*

525 Plates were imaged using a Nikon Ti-2 spinning disk confocal microscope with a stage-
526 top incubator (Tokai Hit), a spinning disk confocal head (Yokogawa; CSU-X1), a Ti2-S-
527 SE stage, multi-point perfect focus system (PFS), an Orca Flash 4.0 CMOS camera,
528 four laser lines (405, 488, 561, 647 nm) with appropriate filter sets (DAPI: 405 nm laser

529 excitation, 455/50 nm emission; GFP: 488 nm laser excitation, 525/36 nm emission;
530 TxRed: 561 nm laser excitation, 605/52 nm emission; SNARF: 561 nm laser excitation,
531 705/72 nm emission; Cy5: 647 nm laser excitation, 705/72 nm emission) were used.
532 Immunofluorescent and live-cell transcriptional reporter images were collected on a 40X
533 oil immersion objective (Nikon, CFI PLAN FLUOR NA 1.30). Photoconversion images
534 were collected on a 60X oil immersion objective (Nikon, CFI PLAN APO OIL 1.40). Live-
535 cell imaging was performed after 24 hours of pHi manipulation. The stage top chamber
536 was equilibrated to 37º C and 5% CO_2 (or 15% CO_2 when capturing experimental
537 images for high pHi) prior to loading plates on microscope.
538
539 *Trypan blue exclusion assay*
540 MDCK cells were plated at $1x10^3$ cells per well in a 24-well plate. Cells were cultured for
541 24 hours after plating before being treated for pHi manipulation as described above.
542 After the 24-hour treatment period, the medium was aspirated, the cells were washed
543 with 1 mL pre-warmed 1X Dulbecco's Phosphate-Buffered Saline (DPBS) (Quality
544 Biological, cat: 114-057-101) prior to trypsinization. Cells were trypsinized in 100 µL of
545 trypsin (Corning, cat: 25-053-CI) for 8-10 minutes to ensure detachment from the plates.
546 Each well then received 100 µL pre-warmed culture medium to inactivate the trypsin
547 and resuspend the trypsinized cells to a single-cell suspension. Immediately before
548 counting cell suspensions, 50 µL of the suspension was mixed with 50 µL trypan blue
549 0.4% solution (Gibco, cat: 15250-061) in a separate Eppendorf tube. Cells were
550 counted using 10 µL of the 1:1 cell suspension:trypan blue mixture in a hemocytometer
551 for healthy (no dye uptake) and unhealthy/dying (blue) cells. Each biological replicate is

552 the average of three wells (technical replicates) plated, treated, and counted on
553 independent days.
554
555 *Population-level pHi measurement using BCECF-AM*
556 MDCK cells were plated at $1x10^3$ cells/mL in 24-well plate 48 hours prior to performing
557 the assay on the plate reader. Cells were treated for pHi manipulation as outlined
558 above. After 24 hours of treatment, 2'-7'-Bis-(2-carboxyethyl)-5-(and-)-
559 carboxyfluorescein, Acetoxymethyl Ester (BCECF-AM) (VWR, 891390244) was
560 prepared as a 100 μM stock solution in 10% DMSO in DPBS. Cells were dye loaded
561 with 1 μM BCECF-AM for 30 minutes in respective culturing conditions. Pre-warmed
562 HEPES-based wash buffer (30 mM HEPES, 145 mM NaCl, 5 mM KCl, 10 mM glucose,
563 1 mM $MgSO_4$, 1mM $KHPO_4$, 2mM $CaCl_2$, pH 7.4) and Nigericin buffer (25 mM HEPES,
564 105 mM KCl, 1 mM $MgCl_2$ supplemented with 10 μM Nigericin (Fisher, N1495)) are
565 prepared the day of the assay. Nigericin buffer is used to prepare three standard buffers
566 with pH values ~7.8, ~7.2 and ~6.5, where pH was accurately recorded to hundredths
567 place for each point and each biological replicate for pHi back-calculation. After dye-
568 loading, cells are washed 3x5minutes with HEPES buffer containing the appropriate
569 treatment at 37º C. Experimental fluorescence intensities were measured on a Biotek
570 Cytation5 plate reader (440ex/535em) and (490ex/535em) with kinetic reads taken
571 every 39 seconds for 7 minutes (11 reads). HEPES wash buffer was aspirated and
572 replaced with Nigericin buffer, pH ~7.8 and incubated for 7 minutes at 37º C before
573 starting the kinetic read. This procedure was repeated for the other two Nigericin
574 buffers. A data reduction step calculates the mean 490/440 intensity for experimental

575 and standardized pH reads where slope and y-intercept are calculated using Nigericin
576 standard buffer pH values to the hundredth place. Population level pHi values are back
577 calculated using experimental ratios and Nigericin standard curve values.
578
579 *Whole-cell lysate preparation & protein quantification*
580 After pHi manipulation (see above section) plates were removed from the incubator and
581 placed on ice. The media was aspirated, and the plates were washed two times with
582 ice-cold DPBS. Plates were wrapped with parafilm and stored at -80º C if not prepared
583 immediately. To washed or thawed plates on ice, 100 µL of lysis buffer (500 mM NaCl,
584 10 mM EDTA, 500mM HEPES-free acid, 10 mM EGTA, 10% Triton X-100, and protease
585 inhibitor cocktail (Pierce™ Protease Inhibitor Tablets, A32965; 1 tablet/50 mL lysis
586 buffer), pH 7.4) was added to each plate. Cells were removed using cell scrapers and
587 transferred to pre-chilled microfuge tubes, briefly vortexed, then incubated on ice for 15
588 minutes. Lysates were centrifuged at 14,000 x g for 15 minutes at 4º C. Clarified lysates
589 were isolated to separate microfuge tubes on ice. The Bradford assay was used to
590 quantify the total protein content of lysates (Bradford, 1976) using Coomassie Protein
591 reagent (Thermo Scientific, cat: 1856209). Lysates were stored at -80º C if not
592 immediately being used for SDS-PAGE sample preparation.
593
594 *Immunoblotting*
595 Protein samples were prepared in 6X Laemilli (reducing) buffer (Thermo Scientific, cat:
596 J61337.AC) and boiled for 10 minutes at 100º C. A total of 5 µg of MDCK lysate was
597 added to each lane for immunoblot analysis. Protein samples were loaded onto 10%

598 SDS-PAGE gels, which were run at 125V and 0.08 Amps for 15 minutes to stack
599 samples. Protein samples were separated by running the gel at 175 V and 0.08 Amps
600 for an hour and a half. Polyvinylidene difluoride (PVDF) membranes were pre-soaked in
601 100% ethanol for 5 minutes and rinsed 3X in water. Wet transfers were performed on
602 ice at a constant amperage of 0.04 A (100V) for an hour and half in transfer buffer (Tris-
603 Glycine buffer, 10% methanol, 0.01% SDS). Membranes were blocked for 1 hour in 5%
604 milk in 1X Tris-buffered Saline + 0.1% Tween® 20 (TBS-T) at room temperature with
605 shaking. Membranes were washed 3x5 min in 1X TBS-T before being cut and incubated
606 with primary antibodies. The following primary antibodies were used: β-catenin (BD
607 Biosciences, 610154; 1:5000 dilution in 3% BSA in 1X TBS-T), plakoglobin (Cell
608 Signaling, 2309S; 1:2000 dilution in 3% BSA in 1X TBS-T) and actin (Santa Cruz, sc-
609 58673; 1:500 diluted in 3% BSA in 1X TBS-T). Primary antibodies were incubated
610 overnight at 4º C with shaking. Primary antibody solutions were removed, and
611 membranes were washed 3x5 minutes in 1X TBS-T before incubating secondary
612 antibodies (Goat anti-mouse/rabbit HRP-conjugated antibodies; 1:10,000 diluted in 5%
613 milk in 1X TBS-T) for 1 hour at room temperature with shaking. Secondary antibody
614 solutions were removed, and membranes were washed 3x5 minutes in 1X TBS-T before
615 being developed using Pierce SuperSignal West Pico PLUS (Thermo Scientific, cat:
616 34580) (β-catenin, actin) or Pierce SuperSignal West Femto PLUS (Thermo Scientific,
617 cat: 34095) (plakoglobin). Chemiluminescence and colorimetric images were acquired
618 using a BioRad ChemiDoc imager.
619

620 *Western Blot Analysis*

621 Raw files were exported from ChemiDoc imager and opened in ImageJ. Band
622 intensities were acquired by densitometry analysis (area under the curve of individual
623 bands in respective lanes). For each replicate blot, target protein intensities were
624 normalized to the intensity of loading controls before normalizing each condition ratio to
625 that of the control within biological replicates.

626

627 *Single-cell pHi calculations using SNARF-AM and confocal microscopy*

628 Cells were plated at $5x10^3$ cells per well (4-well glass bottom dish) or $2\ x10^4$ cells per
629 dish (35 mm dish with 14 mm glass cover slip) in complete medium 48 hours prior to
630 imaging. Cells were treated for pHi manipulation as described above. Fields of view
631 (FOVs) were selected by viewing cells in differential interference contract (DIC). Cells
632 were dye loaded in conditioned media with 10 μM of 5-(and-6)-Carboxy SNARF ™-1
633 Acetoxymethyl Ester, Acetate (Fisher Scientific, cat: C1272) prepared as a 100 μM
634 stock solution dissolved in a 10% DMSO in DPBS for 10 minutes on the microscope
635 stage. Dye-containing media was removed, and plates were washed three times with
636 pre-warmed complete growth medium containing appropriate treatment. A 10-minute
637 equilibration period was used prior to capturing images in SNARF (20% laser power,
638 400 ms), TxRed (20% laser power, 400 ms), and DIC (200 ms) channels for each FOV
639 with five z-stacks (+/- 1 μm; 0.5 μm steps). SNARF dye was calibrated using three pre-
640 warmed Nigericin buffers (as described above). Complete medium was removed after
641 the initial capture and the pH ~7.8 Nigericin buffer was used to wash the plate and
642 incubated for 10 minutes prior to capture. This procedure was repeated for standard

643 points at pH ~7.2 and ~6.5. After data acquisition the NIS-Elements Analysis software
644 was used to define single-cell regions of interest (ROIs) after background subtraction for
645 each channel. The mean fluorescence intensity for each ROI in each channel was
646 exported to Microsoft Excel. Ratios were calculated by dividing the SNARF mean
647 intensity by the TxRed mean intensity for each capture. The three ratios for each
648 nigericin point and their corresponding pH values were used to calculate slope and y-
649 intercept. These values and the experimental ratio of SNARF/TxRed were used to back
650 calculate single-cell pHi values.
651
652 *Immunofluorescent Staining*
653 Cells were cultured in 35 mm imaging dishes containing a 14 mm glass coverslip and
654 plated for experiments 48 hours prior to fixation. Cells were treated for pHi manipulation
655 as described above. Intracellular pH was manipulated for 24 hours before removing
656 culture dishes from the incubator and washing them with ice-cold DPBS. After being
657 washed, cells were fixed in 3.7% paraformaldehyde in DPBS for 10 minutes at room
658 temperature with shaking. The fixative solution was removed, and cells were washed
659 3x2 minutes in DPBS. Cells were permeabilized for 10 minutes at room temperature in
660 a 0.1% Triton X-100 in 1X DBPS. Permeabilization buffer was removed and washed 3x2
661 minutes before blocking for 1 hour at room temperature in a 1% Bovine Serum Albumin
662 (BSA) (Millipore Sigma, cat: 2910-OP) in DPBS solution. The blocking solution was
663 removed and washed 3x2 minutes in DPBS. Primary antibodies (see Immunoblotting
664 methods 1.3.7 for vendor information) were diluted in antibody solution (1% BSA, 0.1%
665 Triton X-100 in DPBS) with the following dilutions: mouse anti-β-catenin (1:200), rabbit

666 anti-plakoglobin (1:400), and rat anti-E-cadherin (1:200). Primary antibody solutions
667 were incubated in dishes at 4º C overnight with rocking. After primary antibody
668 incubation, the plates were washed 3x2 minutes prior to incubating Alexa-Fluor
669 conjugated secondary antibodies diluted 1:1000 in antibody solution for 1 hour at room
670 temperature while being protected from light. Secondary antibody solutions were
671 removed and washed from the plates 3x2 minutes using DPBS. Cells were
672 counterstained with Hoechst dye (DAPI; Thermo Scientific, cat: 62249) diluted 1:10,000
673 in antibody solution for 10 minutes at room temperature protected from light.
674 Counterstain was removed and washed 3x2 minutes in DPBS. Imaging dishes were
675 stored and imaged in DPBS. Image acquisition details are outlined above. Z-stacks
676 were collected 2 μm above and below a relative z-plane that captured the center of the
677 cell determined using the DAPI channel. Nuclear pools of proteins were identified using
678 Nikon Elements Analysis software by auto-detecting individual regions of interest (ROI)
679 in the DAPI channel that represent individual nuclei. Whole cell regions of interest were
680 hand drawn using E-cadherin as a membrane marker to differentiate single-cells,
681 drawing the ROI interior to E-cadherin staining to prevent inclusion of membrane signal.
682 Nuclear ROIs were subtracted from hand-drawn whole cell ROIs to produce cytoplasmic
683 ROIs, excluding both cell membranes and nuclei. The mean intensity for each channel
684 was exported for each z-plane that had the largest mean intensity in the DAPI which
685 indicated the center of the individual cells. Junctional protein levels were quantified
686 using IMARIS software (Oxford Instruments, version 9.5.1) by generating surfaces
687 based on E-cadherin intensity. Mean intensities for all channels within each surface
688 were exported and analyzed for statistical significance using GraphPad Prism software.

689

690 *Cycloheximide chase assay*

691 Cells were plated at $1.5x10^4$ cells per well in 6 well plate 48 hours prior to collecting
692 lysates. 24 hours after plating, cells were treated for pHi manipulation as described
693 above. Stock solutions of cycloheximide (VWR, 9427) were prepared fresh for each
694 experiment. After 20 hours of pHi manipulation, all plates except time-0 samples were
695 treated with 50 µg/mL cycloheximide and returned to the appropriate incubator.
696 Immediately after treatment, lysates from time-0 plates were prepared as described
697 previously and the remaining samples were lysed every 30 minutes for 2.5 hours.
698 Immunoblotting and analysis of β-catenin and actin were performed as described
699 above. The ratio of β-catenin to actin for each time point was normalized to time=0 h
700 within each condition and for each replicate. Normalized data for each biological
701 replicate was imported to Prism where one-phase decay was used to determine half-life
702 values.

703

704 *Quantifying protein degradation and re-localization using mMaple3 constructs via*
705 *photoconversion and confocal microscopy*

706 MDCK cells were seeded at $3x10^6$ cells in 10 cm dishes and allowed to adhere to the
707 dish for 8 hours. 8 hours after seeding, cells were transfected with 15 µg mMaple3
708 containing plasmid (mMaple3 alone, mMaple3-β-catenin WT or H36R) using
709 Lipofectamine 3000 according to the manufacturer's instructions. Transfections
710 proceeded for 18 hours prior to the removal of transfection media, rinsing of the plate
711 with 10 mL of warm DPBS, and addition of 1 mL trypsin. Cells were trypsinized at 37º C

712 for 8-10 minutes. After all the cells were detached, complete medium was added to the
713 dish to create a single cell suspension. Using the transfected single cell suspension, 35
714 mm imaging dishes were seeded at $2.5x10^4$ cell per dish and adhered for 8 hours. After
715 the cells adhered for 8 hours, pHi manipulation was performed as described above.
716 Images were collected as described above. Cell nuclei were visualized via SPY650-
717 DNA (Cytoskeleton, cat. #: CY-SC501) probe that was incubated for 2 hours at 37º C at
718 a 1:1,000 dilution in complete media. Photoconversion was performed using a digital
719 micromirror device (DMD) patterned illumination system (Polygon 4000) at 405 nm. For
720 each experiment, an extra plate was prepared to calibrate the DMD device for a fixed
721 stimulation ROI of 6x16 pixels. Pre-stimulation images were acquired with using GFP
722 (pre-conversion mMaple3; 30% laser power, 500 ms) and Cy5 (DNA; 25% laser power,
723 200 ms), which were used to place the stimulation ROI. Within the Nikon Elements
724 software, an ND Stimulation protocol was used to stimulate at 405 nm within a user-
725 defined stimulation ROI (6x16 pixels) and then acquire images across the entire FOV
726 using TxRed (converted mMaple3; 30% laser, 500 ms). For these experiments, a pre-
727 conversion image was acquired followed by photoconversion of mMaple3 or mMaple3-
728 β-catenin constructs using 405 nm light at 100% LED power for 90 seconds. Then the
729 converted (TxRed) signal was monitored every 30 seconds for 10 minutes post-
730 conversion. ROIs for nuclei and cytoplasm were generated using GFP (unconverted
731 mMaple3) and Cy5 (DNA probe) images and applied to the photoconverted movies to
732 track nuclear and cytoplasmic signal over time. Cytoplasmic tracking data were
733 exported to excel and normalized for mMaple3 and mMaple3-β-catenin -/+ MG132 at
734 t=185 seconds. Normalized traces from individual cell cytoplasmic ROIs were imported

735 to Prism and fit using nonlinear regression comparing one-phase and two-phase decay
736 models with a constrained Y_o equal to 1.0. Two-phase decay models fit mMaple3-β-
737 catenin -/+ MG132 curves significantly better and were used to compare mMaple3 and
738 mMaple3-β-catenin -/+ MG132. Raw cytoplasmic traces for mMaple3-β-catenin under
739 low, control, high pHi conditions were imported to Prism for visualization and nonlinear
740 regression. Comparing goodness of fit between one-phase and two-phase decay
741 models with a constrained Y_o equal to 1.0 showed that two-phase models better
742 represent curves under low and high pHi conditions. Even though the one-phase model
743 was preferred for control conditions, the half-life parameter was nonsensically higher
744 (204-fold higher) whereas the two-phase half-life parameter was only 10% higher
745 compared to previous experiments. For that reason, one-phase decay models were
746 used to compare mMaple3-β-catenin degradation under low, control, and high pHi
747 conditions. Nuclear re-localization was quantified by generating nuclear ROIs based on
748 SPY650-DNA intensity (see above) and quantifying nuclear intensity over the same time
749 course used to monitor cytoplasmic degradation, in matched cells. Nuclear intensity was
750 normalized to t=185 seconds and median traces were imported to Prism and fit using
751 nonlinear regression and a one-phase association model with a constrained Y_o equal to
752 1.0 to account for normalization. Overall nuclear accumulation was readout by
753 comparing plateau values between pHi conditions, where statistical comparison
754 demonstrated that the same plateau value cannot adequately fit each dataset.
755
756 *RNA extraction from MDCK cells*

757 MDCK cells were trypsinized and pellets of $1x10^6$ cells were frozen at -80º C. Pellets
758 were thawed on ice and the QIAGEN RNeasy Plus kit was used to extract total RNA.
759 Yields were quantified using a nanodrop. Extracted RNA was stored at -80º C until used
760 for reverse transcriptase reaction. cDNA was synthesized using 1000 ng extracted RNA
761 and the SuperScript IV reverse transcriptase (Thermo Fisher, cat. # 18090010) following
762 the manufacturer's instructions.
763
764 *Real-time quantitative polymerase chain reaction (RT-qPCR) of endogenous β-catenin*
765 *transcriptional targets*
766 Primers for qPCR (Table 1) were confirmed using standard PCR using DreamTaq
767 master mix (Thermo Fisher, cat: K1082), 500 ng cDNA, and 500 nM forward and
768 reverse primers. qPCR was performed on a BioRad CFX Connect using applied
769 biosystems PowerUp SYBR Green Master Mix (Thermo Fisher Scientific, cat:
770 100029284). Analysis of MYC and SLUG were performed with 500 nM of each primer
771 and 10 ng of cDNA and normalized to RPLP2 using the same concentration of primer
772 and cDNA. Each 20 µL reaction contained 10 µL of SYBR Green, the listed primer and
773 cDNA concentrations, and diluted with water. The thermocycling conditions were as
774 follows: pre-denaturation at 95º C for 2 minutes followed by 40 cycles of denaturation at
775 95º C for 15 sec, annealing at 55º C for 15 sec, and extension at 72º C for 60 sec.
776 Analysis was performed using the $2^{-\Delta\Delta Cq}$ method (Livak and Schmittgen, 2001). Each
777 target was analyzed using technical triplicate (n=3) wells and averaged to obtain
778 biological replicate Cq value relative to the normalizing gene, RPLP2, and each

779 condition was normalized to control. Five biological replicate (N=5) Cq values were
780 averaged to calculate the change in expression of each target relative to control.
781
782 Table 1: Primer sequences used in RT-qPCR

Target	Sequence 5' → 3'
RPLP2-F	GCTACGTCGCCTCCTACCTG
RPLP2-R	GCTCGCTGATGACCTTGTTG
MYC-F	GGTCTTCGGACACGGAGGAG
MYC-R	TGGACGGACAGGATGTACGC
SLUG-F	AGTGATTATTTCCCCATATCTCTATGA
SLUG-R	GTAGTCTTTCCTCTTCATCACTAATGG

783
784 *Single-cell β-catenin transcriptional activity assays using live-cell microscopy*
785 Lentiviral-TOP/FOP-dGFP-reporters (wild-type consensus plasmid TOP: Addgene
786 plasmid #14715; http://n2t.net/addgene:14715 ; RRID:Addgene_14715; inverted
787 consensus plasmid FOP: Addgene plasmid # 14885 ; http://n2t.net/addgene:14885 ;
788 RRID:Addgene_14885) were a gift from Tannishtha Reya. MDCK cells were seeded at
789 $3x10^6$ cells in 10 cm dishes and allowed to adhere to the dish for 8 hours. 8 hours after
790 seeding, cells were transfected with 0 µg (mock transfection) or 15 µg TOP-dGFP-
791 reporter/FOP-dGFP-reporter plasmid using Lipofectamine 3000 according to the
792 manufacturer's instructions. Transfections proceeded for 18 hours prior to the removal
793 of transfection media, rinsing of the plate with 10 mL of warm DPBS, and addition of 1
794 mL trypsin. Cells were trypsinized at 37º C for 8-10 minutes. After all the cells were

795 detached, complete medium was added to the dish to create a single cell suspension.
796 Using the transfected single cell suspension, 35 mm imaging dishes were seeded at
797 $1.5x10^4$ cell per dish and adhered for 8 hours. After the cells adhered for 8 hours, the
798 plating medium was removed and replaced with complete media used for pHi
799 manipulations (see section above) or Wnt stimulation (40 ng/mL (Cf) murine WNT3a
800 (Peprotech; 315-20)). Images were acquired as outlined in the above sections. Cell
801 nuclei and cell membranes were visualized via Hoechst dye (DAPI; Thermo Scientific,
802 cat: 62249; 1:10,000) and CellMask Deep Red (Thermo Fisher, C10046; 1:20,000),
803 respectively, incubated for 15 minutes at 37º C in complete media. Fields of view were
804 selected by visualizing nuclei (DAPI) and images were collected in the DAPI (20% laser
805 power, 400 ms), GFP (30% laser power, 500 ms), Cy5 (20% laser power, 400 ms), and
806 DIC (32.6 DIA, 200 ms) channels. Whole-cell regions of interest (ROIs) were drawn
807 within individual cells using cell mask as a membrane marker and the average GFP
808 intensity for individual cells were exported to Excel. Single-cell intensities that were
809 greater than 2X the average intensity of mock transfected cells was imported to
810 GraphPad Prism for statistical analysis and visualization. None of the cells expressing
811 FOP-dGFP that were analyzed met the 2-fold mock cutoff to be included in the final
812 analysis.
813
814 *Statistics*
815 GraphPad Prism (10.0) was used to prepare graphs and perform statistical comparisons
816 as indicated in each figure legend. Normality tests were performed on all datasets after
817 performing outlier analysis on pooled data (ROUT method; Q=1%), where normally

distributed data is shown with means and non-normally distributed data is shown with medians. “N” indicates the number of biological replicates performed and “n” represents the number of technical replicates or individual measurements collected.

Online Supplementary Materials: Online supplementary materials include Figure S1-S8 and Supplemental Video S1.

Acknowledgements: We would like to thank Tannishtha Reya for TOP/FOP-dGFP-reporter plasmids (TOP: Addgene plasmid #14715; http://n2t.net/addgene:14715 ; RRID:Addgene_14715; FOP: Addgene plasmid # 14885 ; http://n2t.net/addgene:14885 ; RRID:Addgene_14885). We would also like to thank members of the White lab for their helpful conversations and feedback during figure and manuscript preparation. The spinning disk confocal microscope used in this work is a part of the Notre Dame Integrated Imaging Facility (NDIIF).

Author contributions:

Conceptualization: BJC, KAW; Methodology: BJC, KAW; Validation: BJC, KAW; Formal analysis: BJC, KAW; Investigation: BJC; Resources: K.A.W.; Data collection: BJC; Data curation: BJC, KAW; Writing – original draft: BJC; Writing - review & editing: BJC, KAW; Visualization: BJC, KAW; Supervision: BJC, KAW; Project administration: KAW; Funding acquisition: KAW

Competing Interests: Authors declare no competing interests.

841 **Funding:**

842 This work was supported by an National Science Foundation NSF CAREER Award (

843 MCB-2238694) and the Henry Luce Foundation. KAW was additionally supported by the

844 NIH Director's New Innovator Award (1DP2CA260416-01).

845

846 **References**

847 Amith, S.R., J.M. Wilkinson, and L. Fliegel. 2016. Na+/H+ exchanger NHE1 regulation
848 modulates metastatic potential and epithelial-mesenchymal transition of triple-negative
849 breast cancer cells. *Oncotarget*. 7:21091–21113. doi:10.18632/oncotarget.8520.

850 Bradford, M.M. 1976. A rapid and sensitive method for the quantitation of microgram quantities
851 of protein utilizing the principle of protein-dye binding. *Analytical Biochemistry*. 72:248–
852 254. doi:10.1016/0003-2697(76)90527-3.

853 Chen, Y.-T., D.B. Stewart, and W.J. Nelson. 1999. Coupling Assembly of the E-Cadherin/β-
854 Catenin Complex to Efficient Endoplasmic Reticulum Exit and Basal-lateral Membrane
855 Targeting of E-Cadherin in Polarized MDCK Cells. *Journal of Cell Biology*. 144:687–
856 699. doi:10.1083/jcb.144.4.687.

857 Cowin, P., H.-P. Kapprell, W.W. Franke, J. Tamkun, and R.O. Hynes. 1986. Plakoglobin: A
858 protein common to different kinds of intercellular adhering junctions. *Cell*. 46:1063–
859 1073. doi:10.1016/0092-8674(86)90706-3.

860 Daniels, D.L., and W.I. Weis. 2005. β-catenin directly displaces Groucho/TLE repressors from
861 Tcf/Lef in Wnt-mediated transcription activation | Nature Structural & Molecular
862 Biology. *Nature Structural & Molecular Biology*. 12:364–371.

863 Denker, S.P., and D.L. Barber. 2002. Cell migration requires both ion translocation and
864 cytoskeletal anchoring by the Na-H exchanger NHE1. *Journal of Cell Biology*.
865 159:1087–1096. doi:10.1083/jcb.200208050.

866 Dovmark, T.H., M. Saccomano, A. Hulikova, F. Alves, and P. Swietach. 2017. Connexin-43
867 channels are a pathway for discharging lactate from glycolytic pancreatic ductal
868 adenocarcinoma cells. *Oncogene*. 36:4538–4550. doi:10.1038/onc.2017.71.

869 Drees, F., S. Pokutta, S. Yamada, W.J. Nelson, and W.I. Weis. 2005. α-Catenin Is a Molecular
870 Switch that Binds E-Cadherin-β-Catenin and Regulates Actin-Filament Assembly. *Cell*.
871 123:903–915. doi:10.1016/j.cell.2005.09.021.

872 Fevr, T., S. Robine, D. Louvard, and J. Huelsken. 2007. Wnt/β-Catenin Is Essential for Intestinal
873 Homeostasis and Maintenance of Intestinal Stem Cells. *Mol Cell Biol*. 27:7551–7559.
874 doi:10.1128/MCB.01034-07.

875 Frantz, C., A. Karydis, P. Nalbant, K.M. Hahn, and D.L. Barber. 2007. Positive feedback
876 between Cdc42 activity and H+ efflux by the Na-H exchanger NHE1 for polarity of
877 migrating cells. *Journal of Cell Biology*. 179:403–410. doi:10.1083/jcb.200704169.

878 Fukunaga, Y., H. Liu, M. Shimizu, S. Komiya, M. Kawasuji, and A. Nagafuchi. 2005. Defining
879 the roles of β-catenin and plakoglobin in cell-cell adhesion: Isolation of β-
880 catenin/plakoglobin-deficient F9 cells. *Cell Structure and Function*. 30:25–34.
881 doi:10.1247/csf.30.25.

882 Grillo-Hill, B.K., B.A. Webb, and D.L. Barber. 2014. Chapter 23 - Ratiometric Imaging of pH
883 Probes. *In* Methods in Cell Biology. J.C. Waters and T. Wittman, editors. Academic
884 Press. 429–448.

885 Hart, M., J.-P. Concordet, I. Lassot, I. Albert, R. del los Santos, H. Durand, C. Perret, B.
886 Rubinfeld, F. Margottin, R. Benarous, and P. Polakis. 1999. The F-box protein β-TrCP
887 associates with phosphorylated β-catenin and regulates its activity in the cell. *Current*
888 *Biology*. 9:207–211. doi:10.1016/S0960-9822(99)80091-8.

889 He, T.-C., A.B. Sparks, C. Rago, H. Hermeking, L. Zawel, L.T. da Costa, P.J. Morin, B.
890 Vogelstein, and K.W. Kinzler. 1998. Identification of c-MYC as a Target of the APC
891 Pathway. *Science*. 281:1509–1512. doi:10.1126/science.281.5382.1509.

892 Howard, S., T. Deroo, Y. Fujita, and N. Itasaki. 2011. A Positive Role of Cadherin in Wnt/β-
893 Catenin Signalling during Epithelial-Mesenchymal Transition. *PLOS ONE*. 6:e23899.
894 doi:10.1371/journal.pone.0023899.

895 Huber, A.H., D.B. Stewart, D.V. Laurents, W.J. Nelson, and W.I. Weis. 2001. The Cadherin
896 Cytoplasmic Domain Is Unstructured in the Absence of β-Catenin: A POSSIBLE
897 MECHANISM FOR REGULATING CADHERIN TURNOVER *. *Journal of Biological*
898 *Chemistry*. 276:12301–12309. doi:10.1074/jbc.M010377200.

899 Kao, S.-H., W.-L. Wang, C.-Y. Chen, Y.-L. Chang, Y.-Y. Wu, Y.-T. Wang, S.-P. Wang, A.I.
900 Nesvizhskii, Y.-J. Chen, T.-M. Hong, and P.-C. Yang. 2015. Analysis of Protein Stability
901 by the Cycloheximide Chase Assay. *Bio Protoc*. 5:e1374. doi:10.21769/BioProtoc.1374.

902 Krieghoff, E., J. Behrens, and B. Mayr. 2006. Nucleo-cytoplasmic distribution of β-catenin is
903 regulated by retention. *Journal of Cell Science*. 119:1453–1463. doi:10.1242/jcs.02864.

904 Larsen, A.M., N. Krogsgaard-Larsen, G. Lauritzen, C.W. Olesen, S. Honoré Hansen, E.
905 Boedtkjer, S.F. Pedersen, and L. Bunch. 2012. Gram-Scale Solution-Phase Synthesis of
906 Selective Sodium Bicarbonate Co-transport Inhibitor S0859: in vitro Efficacy Studies in
907 Breast Cancer Cells. *ChemMedChem*. 7:1808–1814. doi:10.1002/cmdc.201200335.

908 Lee, D.H., and A.L. Goldberg. 1996. Selective Inhibitors of the Proteasome-dependent and
909 Vacuolar Pathways of Protein Degradation in Saccharomyces cerevisiae. *Journal of*
910 *Biological Chemistry*. 271:27280–27284. doi:10.1074/jbc.271.44.27280.

911 Lewis, J.E., J.K. Wahl, K.M. Sass, P.J. Jensen, K.R. Johnson, and M.J. Wheelock. 1997. Cross-
912 Talk between Adherens Junctions and Desmosomes Depends on Plakoglobin. *J Cell Biol*.
913 136:919–934.

914 Liu, Y., E. Reyes, D. Castillo-Azofeifa, O.D. Klein, T. Nystul, and D.L. Barber. 2023.
915 Intracellular pH dynamics regulates intestinal stem cell lineage specification. *Nat*
916 *Commun*. 14:3745. doi:10.1038/s41467-023-39312-9.

917 Liu, Y., K.A. White, and D.L. Barber. 2020. Intracellular pH Regulates Cancer and Stem Cell
918 Behaviors: A Protein Dynamics Perspective. *Frontiers in Oncology*. 10.

919 Livak, K.J., and T.D. Schmittgen. 2001. Analysis of relative gene expression data using real-time
920 quantitative PCR and the 2(-Delta Delta C(T)) Method. *Methods*. 25:402–408.
921 doi:10.1006/meth.2001.1262.

922 MacDonald, B.T., K. Tamai, and X. He. 2009. Wnt/β-Catenin Signaling: Components,
923 Mechanisms, and Diseases. *Developmental Cell*. 17:9–26.
924 doi:10.1016/j.devcel.2009.06.016.

925 Martínez-Estrada, O.M., A. Cullerés, F.X. Soriano, H. Peinado, V. Bolós, F.O. Martínez, M.
926 Reina, A. Cano, M. Fabre, and S. Vilaró. 2006. The transcription factors Slug and Snail
927 act as repressors of Claudin-1 expression in epithelial cells1. *Biochemical Journal*.
928 394:449–457. doi:10.1042/BJ20050591.

929 McEvoy, A.L., H. Hoi, M. Bates, E. Platonova, P.J. Cranfill, M.A. Baird, M.W. Davidson, H.
930 Ewers, J. Liphardt, and R.E. Campbell. 2012. mMaple: A Photoconvertible Fluorescent
931 Protein for Use in Multiple Imaging Modalities. *PLOS ONE*. 7:e51314.
932 doi:10.1371/journal.pone.0051314.

933 Moon, J.H., S.H. Lee, and Y.C. Lim. 2021. Wnt/β-catenin/Slug pathway contributes to tumor
934 invasion and lymph node metastasis in head and neck squamous cell carcinoma. *Clin Exp*
935 *Metastasis*. 38:163–174. doi:10.1007/s10585-021-10081-3.

936 Morgan, R.G., J. Ridsdale, M. Payne, K.J. Heesom, M.C. Wilson, A. Davidson, A. Greenhough,
937 S. Davies, A.C. Williams, A. Blair, M.L. Waterman, A. Tonks, and R.L. Darley. 2019.
938 LEF-1 drives aberrant β-catenin nuclear localization in myeloid leukemia cells.
939 *Haematologica*. 104:1365–1377. doi:10.3324/haematol.2018.202846.

940 Mukherjee, A., N. Dhar, M. Stathos, D.V. Schaffer, and R.S. Kane. 2018. Understanding How
941 Wnt Influences Destruction Complex Activity and β-Catenin Dynamics. *iScience*. 6:13–
942 21. doi:10.1016/j.isci.2018.07.007.

943 Nusse, R. 2008. Wnt signaling and stem cell control. *Cell Res*. 18:523–527.
944 doi:10.1038/cr.2008.47.

945 Nusse, R., and H. Clevers. 2017. Wnt/β-Catenin Signaling, Disease, and Emerging Therapeutic
946 Modalities. *Cell*. 169:985–999. doi:10.1016/j.cell.2017.05.016.

947 Perez-Moreno, M., and E. Fuchs. 2006. Catenins: Keeping Cells from Getting Their Signals
948 Crossed. *Developmental Cell*. 11:601–612. doi:10.1016/j.devcel.2006.10.010.

949 Reya, T., A.W. Duncan, L. Ailles, J. Domen, D.C. Scherer, K. Willert, L. Hintz, R. Nusse, and
950 I.L. Weissman. 2003. A role for Wnt signalling in self-renewal of haematopoietic stem
951 cells. *Nature*. 423:409–414. doi:10.1038/nature01593.

952 Roura, S., S. Miravet, J. Piedra, A.G. de Herreros, and M. Duñach. 1999. Regulation of E-
953 cadherin/Catenin Association by Tyrosine Phosphorylation *. *Journal of Biological*
954 *Chemistry*. 274:36734–36740. doi:10.1074/jbc.274.51.36734.

955 Shcherbakova, D.M., and V.V. Verkhusha. 2014. Chromophore chemistry of fluorescent proteins
956 controlled by light. *Current Opinion in Chemical Biology*. 20:60–68.
957 doi:10.1016/j.cbpa.2014.04.010.

958 Simcha, I., M. Shtutman, D. Salomon, J. Zhurinsky, E. Sadot, B. Geiger, and A. Ben-Ze'ev.
959 1998. Differential nuclear translocation and transactivation potential of β- Catenin and
960 plakoglobin. *Journal of Cell Biology*. 141:1433–1448. doi:10.1083/jcb.141.6.1433.

961 Spear, J.S., and K.A. White. 2023. Single-cell intracellular pH dynamics regulate the cell cycle
962 by timing the G1 exit and G2 transition. *Journal of Cell Science*. 136:jcs260458.
963 doi:10.1242/jcs.260458.

964 Tafech, A., P. Jacquet, C. Beaujean, A. Fertin, Y. Usson, and A. Stéphanou. 2023.
965 Characterization of the Intracellular Acidity Regulation of Brain Tumor Cells and
966 Consequences for Therapeutic Optimization of Temozolomide. *Biology*. 12:1221.
967 doi:10.3390/biology12091221.

968 Tetsu, O., and F. McCormick. 1999. β-Catenin regulates expression of cyclin D1 in colon
969 carcinoma cells. *Nature*. 398:422–426. doi:10.1038/18884.

970 Ulmschneider, B., B.K. Grillo-Hill, M. Benitez, D.R. Azimova, D.L. Barber, and T.G. Nystul.
971 2016. Increased intracellular pH is necessary for adult epithelial and embryonic stem cell
972 differentiation. *Journal of Cell Biology*. 215:345–355. doi:10.1083/jcb.201606042.

973 Valenta, T., G. Hausmann, and K. Basler. 2012. The many faces and functions of β-catenin.
974 *EMBO J*. 31:2714–2736. doi:10.1038/emboj.2012.150.

975 Van Der Wal, T., and R. Van Amerongen. 2020. Walking the tight wire between cell adhesion
976 and WNT signalling: A balancing act for β-catenin: A balancing act for CTNNB1. *Open*
977 *Biology*. 10. doi:10.1098/rsob.200267.

978 Vleminckx, K., R. Kemler, and A. Hecht. 1999. The C-terminal transactivation domain of β-
979 catenin is necessary and sufficient for signaling by the LEF-1/β-catenin complex in
980 Xenopus laevis. *Mechanisms of Development*. 81:65–74. doi:10.1016/S0925-
981 4773(98)00225-1.

982 Wang, S., J.R. Moffitt, G.T. Dempsey, X.S. Xie, and X. Zhuang. 2014. Characterization and
983 development of photoactivatable fluorescent proteins for single-molecule-based
984 superresolution imaging. *Proceedings of the National Academy of Sciences of the United*
985 *States of America*. 111:8452–8457. doi:10.1073/pnas.1406593111.

986 White, K.A., B.K. Grillo-Hill, and D.L. Barber. 2017. Cancer cell behaviors mediated by
987 dysregulated pH dynamics at a glance. *Journal of Cell Science*. 130:663–669.
988 doi:10.1242/jcs.195297.

989 White, Katharine A.; Grillo-Hill, Bree K.; Esquivel, Mario; Peralta, Jobelle; Bui, Vivian N.;
990 Chire, Ismahan; Barber, D.L. 2018. β-Catenin is a pH sensor with decreased stability at
991 higher intracellular pH. *Journal of Cell Biology*. 217:3965–3976.
992 doi:10.1083/jcb.201712041.

993 Wickline, E.D., P.K. Awuah, J. Behari, M. Ross, D.B. Stolz, and S.P.S. Monga. 2011.
994 Hepatocyte γ-catenin compensates for conditionally deleted β-catenin at adherens
995 junctions. *Journal of Hepatology*. 55:1256–1262. doi:10.1016/j.jhep.2011.03.014.

996 Wodarz, A., and R. Nusse. 1998. Mechanisms of Wnt Signaling in Development. *Annual Review*
997 *of Cell and Developmental Biology*. 14:59–88. doi:10.1146/annurev.cellbio.14.1.59.

998 Yi, H., G. Li, Y. Long, W. Liang, H. Cui, B. Zhang, Y. Tan, Y. Li, L. Shen, D. Deng, Y. Tang,
999 C. Mao, S. Tian, Y. Cai, Q. Zhu, Y. Hu, W. Chen, and L. Fang. 2020. Integrative multi-
1000 omics analysis of a colon cancer cell line with heterogeneous Wnt activity revealed
1001 RUNX2 as an epigenetic regulator of EMT. *Oncogene*. 39:5152–5164.
1002 doi:10.1038/s41388-020-1351-z.

1003 Yost, C., M. Torres, J.R. Miller, E. Huang, D. Kimelman, and R.T. Moon. 1996. The axis-
1004 inducing activity, stability, and subcellular distribution of beta-catenin is regulated in
1005 Xenopus embryos by glycogen synthase kinase 3. *Genes Dev.* 10:1443–1454.
1006 doi:10.1101/gad.10.12.1443.

1007 Zhang, L., N.G. Gurskaya, E.M. Merzlyak, D.B. Staroverov, N.N. Mudrik, O.N. Samarkina,
1008 L.M. Vinokurov, S. Lukyanov, and K.A. Lukyanov. 2007. Method for real-time
1009 monitoring of protein degradation at the single cell level. *BioTechniques*. 42:446–450.
1010 doi:10.2144/000112453.

1011 Zhou, J., J. Qu, P.Y. Xian, K. Graber, L. Huber, X. Wang, A.M. Gerdes, and F. Li. 2007.
1012 Upregulation of γ-catenin compensates for the loss of β-catenin in adult cardiomyocytes.
1013 *American Journal of Physiology - Heart and Circulatory Physiology*. 292:270–276.
1014 doi:10.1152/ajpheart.00576.2006.

1015